

# Pattern Prediction and Passive Bandwidth Management for Hand-Over Optimization in QoS Cellular Networks with Vehicular Mobility

Peppino Fazio, Mauro Tropea, Floriano De Rango, *Member, IEEE*, Miroslav Voznak, *Member, IEEE*

**Abstract**— In wireless networking the main desire of end-users is to take advantage of satisfactory services, in terms of QoS, especially when they pay for a required need. Many efforts have been made to investigate how the continuity of services can be guaranteed in QoS networks, where users can move from one cell to another one. The introduction of a prediction scheme with passive reservations is the only way to face this issue; however, the deployment of in-advance bandwidth leads the system to waste resources. This work consists of two main integrated contributions: a new pattern prediction scheme based on a distributed set of Markov chains, in order to handle passive reservations, and a statistical bandwidth management algorithm for the reduction of bandwidth wastage. The result of the integration is the Distributed Prediction with Bandwidth Management Algorithm (DPBMA) that is independent from the considered technology and the vehicular environment. Several simulation campaigns were conducted in order to evaluate the effectiveness of the proposed idea. It was also compared with other prediction schemes, in terms of system utilization, accuracy, call dropping and call blocking probabilities.

**Index Terms**— Bandwidth, Hand-over management, Markov, Mobility, Passive, Pattern, Prediction, Quality of Service, Resource Reservation, Optimization, Wireless Networks

## I. INTRODUCTION

IN recent years, mobile computing has become very popular with a rapid and emerging growth of Quality of Service (QoS) applications dedicated, mainly, to comfort and reliability. The congestion level, offered in a cellular scenario, may vary from one coverage area to another. When mobile hosts make hand-overs among different coverage areas, they may find scarce resources in the new locations, with high Call Dropping Probability (CDP) values (or heavy degradations). To the best of our knowledge, there is only one way to ensure QoS and service continuity to mobile users: making a bandwidth reservation over all the cells that a Mobile Host (MH) will visit during its active connection. There are many

protocols that can ensure in-advance reservations like Next Step In Signaling (NSIS) [1], Dynamic ReSerVation Protocol (DSRV) [2] and Mobile ReSerVation Protocol (MRSVP) [3], but a prediction scheme is mandatory, in order to know which coverage cells a user will probably visit during its Call Holding Time (CHT). It is essential to underline that the proposed idea does not depend on the adopted signaling protocol: MRSVP can be employed as well as DRSVP or NSIS. In addition, our attention does not focus on the hand-off time (detection, search, and execution phases) for changing the coverage area, but rather on ensuring that there will be sufficient resources in the new coverage cell. The first contribution of the paper is the proposal of a markovian cell prediction algorithm. The second effort of this paper consists in the enhancement of the pre-reservation phase, integrating it with a time-multiplexing algorithm, in order to optimize the system utilization and to reduce the CDP. In addition, since the mobility model has a heavy impact on the obtained results, we employed the Citymob for Roadmaps (C4R) mobility generator [4], that can extract mobility patterns from real roadmaps. The strength of the proposed algorithm, called Distributed Prediction with Bandwidth Management Algorithm (DPBMA), also lies in its independence from the specific coverage technology. The rest of the paper is organized as follows: section II gives an overview of the existing related work, section III describes the proposed scheme in five detailed subsections, section IV shows simulations results then section V concludes the paper.

## II. RELATED WORK AND CONTRIBUTIONS

Mobility and resource management is critical for providing QoS guarantees in wireless networks, therefore it is very important to accurately describe movement patterns of mobile users in wireless cells, especially when prediction is needed.

In [5] Si et al. propose a mobility prediction scheme for cellular networks, based on the analysis of personal mobility in large spatial and temporal scales. The authors stated that the Hidden Markov Model (HMM) fits system modeling and an improved algorithm is proposed to overcome possible calculating defects, demonstrating how HMM is efficient and accurate if adopted in a factual communication system. In [6] the authors proposed a new prediction scheme for analyzing time behavior in real deployment, obtaining strong results in terms of accuracy and energy consumption and solving the problem of continuous sensing in real deployments. In [7] the authors optimize system parameters in terms of CDP and Call Blocking Probabilities (CBP), introducing a prediction

Submitted on

Peppino Fazio is with the University of Calabria, D.I.M.E.S., Via Bucci 41/C, 87036 Arcavacata di Rende (CS) (e-mail: pfazio@dimes.unical.it).

Mauro Tropea is with the University of Calabria, D.I.M.E.S., Via Bucci 41/C, 87036 Arcavacata di Rende (CS) (e-mail: mtropea@dimes.unical.it).

Floriano De Rango is with the University of Calabria, D.I.M.E.S., Via Bucci 41/C, 87036 Arcavacata di Rende (CS) (e-mail: derango@dimes.unical.it).

Miroslav Voznak is with the Technická Univerzita of Ostrava, 17 Listopadu 15/2172,70833 Ostrava-Poruba (e-mail: miroslav.voznak@vsb.cz).

algorithm based on data mining approaches, in order to implement a distributed Call Admission Control (CAC) scheme, also considering the throttle flag as an indication of the usage of each cell. The authors of [8] considered telecom's mobility management for mobile users' movement monitoring, giving the possibility to evaluate the probability that a person will move from a location to another one after a certain amount of time. The authors illustrate how to manage the available data, provided by telecommunications companies, to derive the desired information, by employing the theory of Little's Law. The authors of [9] propose a new framework to estimate service patterns and to track mobile users, basing decisions on historical records and predictive patterns of mobile users allowing estimation of the next cells into which a mobile user will possibly move. In [10] the authors make a contribution to WLAN infrastructure planning, basing their decisions on mobility prediction: they propose a new method for feature extraction with a novel neural network classifier based on a hidden genetic algorithm. Further, in [11] the authors compared three Lempel-Ziv (LZ) prediction algorithms, analyzing in detail two independent phases (tree updating and probability calculation). They concluded that active LZ updating schemes achieve the highest hit rate, at the cost of a higher memory consumption, while the best probability calculation method is the Prediction with Partial Matching (PPM). In [12], [13] the authors propose an in-depth overview on centralized Markov prediction schemes, providing good detail on this topic in wireless networks. They considered the classical approach of the discrete sequence prediction problem, outlining the power of Markov predictors in this field of research. The authors show the strength of the considered schemes, making a comparison between them, with a maximum accuracy of 54%. Also in [14] a comparison is made among different orders of Markov chains, arriving at a prediction accuracy of 65%-70% in the average case. In our previous works, such as [15] and [16], a prediction technique based on the Cell Stay Time (CST) evaluation of a mobile user was proposed. A formula that relates cell coverage radius and mobility behavior is used and resource reservation techniques were proposed, thus, it is possible to evaluate the number of coverage cells that users will visit during their CHT. To the best of our knowledge, regarding the mentioned works, most of the existing prediction schemes are aimed at the prediction of a single next-cell and do not introduce bandwidth multiplexing. Other works predict future locations by considering users' practices during the day and do not take into account the geographical morphology of the considered region, in terms of roads and traffic trends. In general, they guarantee neither a complete service continuity nor a good level of system utilization. In this work, instead, a distributed prediction algorithm is proposed. In particular, the main contributions of our work are:

- Implementation of a distributed approach (instead of a centralized one), in which each coverage cell uses a particular Finite State Markov Chain (FSMC) in order to describe and predict local host movements. Each chain is "tuned" based on the particular coverage region, by the statistical analysis of the number of roads involved in the cell, in addition to the observation of users movements.

Considering one predictor for the whole network has many advantages, but also some drawbacks: the training phase is flexible, as it is based on the observation of complete mobile movements during active connections. On the other side, cell identifiers resume user mobility, and this causes a loss of information about the area morphology and mobility behaviors. Distributed predictors, instead, give the opportunity of taking into account local mobility behaviors of mobile hosts, analyzing geographical morphology during the training phase. Our proposal is based on the statistical analysis of local host movements along urban roads and prediction error is not cumulative: with a single predictor for the whole system, accuracy decreases if the predicted sequence is longer. With a distributed approach, a local decision is affected only by the error committed for the current prediction and does not depend on previous errors;

- Introduction of a roads compression approach based on dynamic programming: in our previous works we considered only one possible hand-over direction for neighboring cells; in order to avoid losing information about user road utilization preferences, taking them into account is useful (as we will demonstrate later). In addition, in order to avoid the management of a larger number of roads, a compression scheme has been adopted, reducing the number of roads and minimizing the approximation error;
- FSMCs training by taking into account local trajectories (belonging to the associated coverage cell); each predictor is specialized for the specific coverage area, with different traffic densities, in terms of roads, road populations, moving directions and so on; mobility has been generated by considering real maps and not synthetic models;
- Statistical analysis of space/time user behaviors is conducted; in particular, the CST random variable is deeply observed in the dynamics of each cell, giving the possibility to know users time dynamics a-priori. Thus, passive bandwidth can be "recycled" in order to reach a higher resource utilization and a reduction of the prediction error;
- Differently from most of the existing centralized schemes, our distributed proposal aims at making a totally in-advance reservation, also guaranteeing service continuity (in terms of bandwidth availability) for non-tolerant applications, optimizing system performance concerning CDP;
- Our proposal is completely independent from the considered signaling protocol (like one of the protocols in [1], [2] or [3]), mobility model or coverage technology and it does not need any information about user habits (like wake-up times, working hours, etc.).

### III. SUITABLE ENVIRONMENTS, PROBLEM STATEMENT AND SYSTEM MODELING

We briefly present how a generic reservation protocol makes passive reservations through signaling. Then, the way we used to model the system through FSMCs is described and, finally, we introduce the concept of time multiplexing of passive resources. Table I summarises the main notations, concepts and abbreviations used in the proposal.

TABLE I. MAIN ABBREVIATIONS, SYMBOLS AND NOTATIONS.

$C$	Set of network cells
$c$	Number of considered network cells equal to $\ C\ $
$c_t$	$t$ -th cell of the system belonging to $C$ , $1 \leq t \leq c$
$n_t$	Number of edges/directions of the $t$ -th cell ( $c_t$ )
$r_t$	Radius of the $t$ -th regular coverage area
$S'_{ho}$	Set of possible hand-off directions of cell $c_t$
$d_j$	$j$ -th direction of $S'_{ho}$ (with fixed $t$ )
$RD_{dj}$	$j$ -th roads set, associated to $d_j$ with $\ RD_{dj}\ =J$
$rd_{djk}$	$k$ -th road belonging to $RD_{dj}$
$\lambda_j$	Compression factor for cell $t$ and side $j$
$T_{dj}$	Array representing the CBT associated to $RD_{dj}$
$t_k$	$k$ -th element of $T_{dj}$ , obtained by compression
$M_j$	Partition vector for $c_t$ and side $j$
$\mu_{jk}$	$k$ -th element of the partition set for cell $t$ and side $j$
$\Omega$	Set of possible Markov states for cell $c^t$
$s_{jk}$	$k$ -th state of side $j$ for the Markov model of $c_t$ (fixed $t$ )
$\Pi$	Set of Markov transition probabilities for $c_t$
$\pi_{j_1k_1 \rightarrow j_2k_2}$	Transition probability from $s_{j_1k_1}$ to $s_{j_2k_2}$
$\sigma$	Initial probability array for $c_t$
$\sigma_{jk}$	Initial probability for state $s_{jk}$
$ST^t$	States sojourn times array for $c_t$
$f_{jk}$	State sojourn time pdf for state $s_{jk}$ of $c_t$
$t_{in}(\alpha)$ , $t_{out}(\alpha)$	$\alpha$ -th hand-in and hand-out times for $c_t$
$\tau'(\alpha)$	CST realization for $c_t$ and $\alpha$ -th hand-over

All requests are subject to an admission control policy on all the involved cells. When a user moves from one coverage area to another one, a reservation switch manages the hand-off event: the reserved resources in the old access point are released and the passive resources can be assigned by switching to an active reservation. Generally, a session starts with the active service request performed by a MH on its active cell and, if enough resources are available, passive reservations are made on the future cells. Message exchanges will be described in depth in subsection III.D. Our proposal is suitable for many technologies: cellular environments [18], especially from 3G to 4G, could benefit from our prediction scheme, as well as more recent WLAN families [19]. The table below gives an idea of some of the main characteristics of the suitable technologies.

TABLE II. SOME SUITABLE TECHNOLOGIES FOR MOBILITY PREDICTION.

	2G	3G	4G	802.11ac
Medium Access	TDMA	WIDE CDMA	OFDM/ SC-FDMA	OFDM
Channel Bandwidth (MHz)	0.2	5	1.5-20	20/40/ 80/160
Carrier Frequency (MHz)	900/ 1800	2000	900/1800 - 2600	5000
Max. Coverage Radius (km)	35	0.1-8	$\approx 1-2$	$\approx 0.015-0.030$

The application of the proposed idea is very easy in the case of a big provider, since they have access to their own mobility data. However, with all the features and services offered by new technologies [14], [24], [35], it can also be applied to low-scale WLAN environments, at the cost of an appropriate device configuration.

#### A. Morphology adaptation and roads compression

We considered a generic Geographical Region ( $GR$ ) covered by a number of cells equal to  $c$ . Let  $C$  be the set of coverage cells of the considered wireless network,  $C=\{c_1, c_2, \dots, c_c\}$  with  $\|C\|=c$ . First, we will analyze the

structure of the cellular system for a regular (ideal) structure, then we will take into account the real coverage, where the shape of the cells is neither regular nor the same for all.

#### 1) Regular and irregular coverages

For each cell  $c_t \in C$ ,  $1 \leq t \leq c$ , with a coverage radius  $r_t$ , a set of neighboring cells  $Adj(c_t)$  can be defined, on the basis of network topology and cell adjacencies. As in the classical treatment, a circular coverage cell can be approached with a  $n$ -edge regular polygon and, considering  $n=6$ , coverage cells are represented by regular hexagonal areas, as approached in [20]. Differently from that work, we will show how considering only  $n=6$  (without considering additional angles), the model suffers a certain error in further prediction making; therefore, more granularity is required, without increasing computational complexity, to adapt the local approximation model to the morphology of the covered region. Let  $GR_x \cdot GR_y$  be the area of the considered region  $GR$ . We started our modeling by assuming that  $r_t=R \forall c_t \in C$  with a regular coverage. When considering real coverage areas, we had to take into account that cellular shapes are affected by different factors, such as site availability, topography and traffic density [21]. Different studies in literature have shown that this problem can be well approached by Voronoi's theory [22]. It gives the opportunity of obtaining irregular convex polygons, able to approximate real coverage regions: for each  $c_t \in C$  there will be an associated value  $n_t$ , indicated with  $n_t$ , representing the number of sides ( $n$  cannot be defined a-priori, because it varies for each cell, depending on the particular shape). So, to overcome the inaccuracy of the classical regular model, Voronoi diagrams are considered for tessellation and system optimization. Let  $\|a-b\|$  denote the Euclidean distance between points  $a, b$  in a plane  $PL \in R^2$  and  $A=\{a_1, a_2, \dots, a_s\}$  a set of  $s$  points. Then, the Voronoi diagram is defined as a subdivision of  $PL$  into  $s$  corresponding polygonal regions  $PL_v$ ,  $v=1, 2, \dots, s$ , such that for each point  $b \in PL$ , it is verified that:

$$\|a_i - b\| < \|a_j - b\|, \quad i, j = 1, 2, \dots, s, \quad i \neq j \quad (1)$$

This yields a plane tessellation, based on convex polygons around the points in the defining point set  $A$ , where any point within a polygon  $PL_j$  is closer to the corresponding point  $a_j$  than to any other points in  $A$ . Assuming that radio signal strength drops in relation to distance, as stated in [21], [22],  $A$  can represent site locations, considering the Voronoi regions as network cells. In this work, we are not interested in deriving a Voronoi/Delaunay diagram from regular coverage: this issue has been extensively studied in literature [21], [22], [23]. We will consider, instead, how our proposed idea performs when irregular shapes are considered for cellular coverage.

#### 2) Roads compression through Run-Length Coding (RLC)

At this point, it is necessary to make some considerations about roads topology. In our previous works [16], [17], [20], [24] we did not differentiate the model based on road densities. For each cell  $c_t \in C$  a set  $S'_{ho}$  of  $n_t$  movement directions  $d_1 \dots d_{n_t}$  can be introduced. For the regular case,  $n_t=n \forall c_t \in C$ , where  $d_j = \theta(2j-1)/2$  rad.,  $\theta = 2\pi/n$  rad. and  $j=1 \dots n$  (the  $j$ -th side of the hexagon), so  $S_{ho}=\{d_1, \dots, d_n\}$  and  $\|S_{ho}\|=n$ . For the irregular case, we can only write that  $\|S'_{ho}\|=n_t \forall c_t \in C$ . In this work  $\|Adj(c_t)\|=\|S'_{ho}\|=n_t, \forall c_t \in C$ . Referring to fig. 1 and considering the regular case, we can observe how a

cell  $c_i \in C$ , on the basis of the value of  $r_i$ , can manage a different number of roads: e.g., considering cells  $c_1, c_2 \in C$ , that cover real geographical areas (two locations of a city in southern Italy are considered), we can immediately observe how the number of possible hand-over roads for  $c_2$  (three sides on a total of six have only one possible direction for hand-over) are lesser than for  $c_1$  (the crosses on the hexagonal sides represent some of the possible hand-in/hand-out points, i.e. intersections among roads and cell sides).

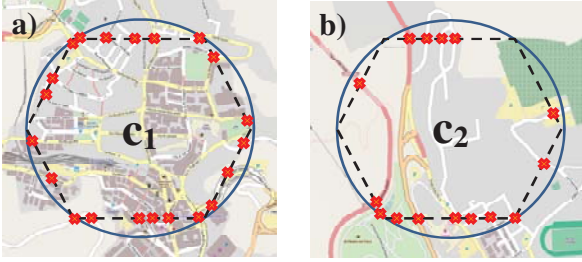


Fig. 1. Different road densities for different coverage cells  $c_1$  and  $c_2$ .

For this reason, the model proposed in our previous works has been particularized for each geographical morphology, in order to take into account different probabilities of handing-over from/to different roads belonging to the same  $d_j \in S_{ho}$ . The main idea is to extend the number of states of the model in order to take into account all the possible crossing directions; on the other hand, model complexity cannot be increased indefinitely, so a correct trade-off should be found, aggregating, when possible, road information belonging to users mobility. For this aim, we considered the RLC approach of [25], in which an input sequence of a certain size is divided into a lower number of sub-sequences, each one represented by the average value. The obtained partitioning minimizes the approximation error. The way to apply this approach to our model is now described. Let us assume that each coverage node (Access Point, Base Station, etc.) is able to recognize the direction from which a MH enters or leaves the cell (Direction-Of-Arrival - DoA, Angle of Arrival - AoA, location or tracking algorithms are present in the literature, depending on the adopted technology [26]). So, referring to a generic coverage cell  $c_i \in C$ , for each  $d_j \in S_{ho}$  we can define a set of roads  $RD_{d_j} = \{rd_{d_{j1}}, rd_{d_{j2}}, \dots, rd_{d_{jJ}}\}$  where  $rd_{d_{jk}} \in [0, 2\pi]$ ,  $k=1, \dots, d_j, ||RD_{d_j}||=J$ .

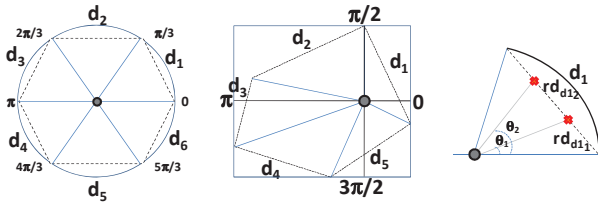


Fig. 2. Cell directions subdivision for regular (left) and irregular (center) shapes and intersection degrees determination (right).

From fig. 2 it can be seen how for each  $d_j \in S_{ho}$  which represents the ‘‘average’’ direction associated to side  $j$ , the lower and upper bounds can be determined, so each  $rd_{d_{jk}} \in RD_{d_j}$  belongs to that interval. Figure 2 shows, on the right, how the angles of road intersections can be determined. Now we focus our attention on the generic  $j$ -th side of cell  $c_i \in C$ , in order to introduce the way we optimized the number of states of the model. Given the sequence of roads/angles  $RD_{d_j} = \{rd_{d_{j1}},$

$rd_{d_{j2}}, \dots, rd_{d_{jJ}}\}$ , with  $||RD_{d_j}||=J$  and a compression factor ( $cf$ )  $\lambda$  (with  $\lambda \leq J$ ), the set  $RD_{d_j}$  has to be divided into  $\lambda$  sub-sequences and each of them has to be replaced with its average value. We followed the approach of [25], which is able to solve a subclass of the RLC scheme, for error minimization in a polynomial time, using a simplified dynamic programming approach.

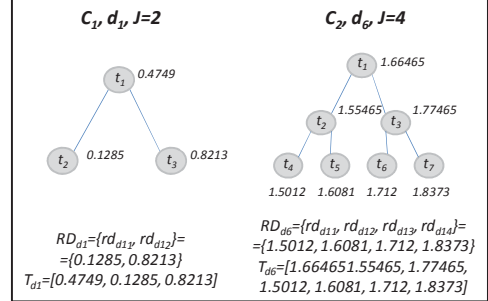


Fig. 3. CBTs and related arrays example for two different directions.

In particular, each  $rd_{d_{jk}} \in RD_{d_j}$  is associated to the terminal nodes of the base level of a Compact Binary Tree (CBT), composed by  $2 \cdot J - 1$  nodes, assuming that  $J=2^l$ . The CBT is represented by an array of the form  $T_{d_j}=[t_1, t_2, \dots, t_{2^l-1}]$ , where each element is associated to a node: the last  $J$  elements store the elements of  $RD_{d_j}$ , while each  $t_k$ , with  $k < J$ , has two children  $t_{2k}$  and  $t_{2k+1}$  and  $2^{h_k}$  descendents, with  $h_k = l_j - \lfloor \log_2 k \rfloor$ , which represents a subsequence  $S_k$  of the input sequence:

$$S_k = \{t_h \mid t_h = rd_{d_{j_{h-k}}}\} \text{ and } k \cdot 2^{h_k} \leq h < (k+1) \cdot 2^{h_k}. \quad (2)$$

In addition  $t_k = (t_{2k} + t_{2k+1})/2 = \mu_k$ . Considering cells  $c_1$  and  $c_2$  in fig. 1 and directions  $d_1$  and  $d_6$  respectively, fig. 3 shows the CBTs and the related arrays. With the approach of [25], the problem is solved by minimizing the quantity  $ERR(k, \lambda)$ , representing the error of compressing the road subsequence  $S_k$  using  $\lambda$  values:

$$ERR(k, \lambda) = \begin{cases} \varepsilon_k & \lambda = 1 \\ \min_{1 \leq p < \lambda} [ERR(2k, p) + ERR(2k+1, \lambda - p)] & \lambda > 1 \\ 0 & \lambda > 2^{h_k} \end{cases} \quad (3)$$

where  $\varepsilon_k$  is the mean square error committed with compression of road subsequence  $S_k$  with a single value:

$$\varepsilon_k = \frac{1}{\|S_k\|} \sum_{r_{d_{jk}} \in S_k} (\mu_k - rd_{d_{jk}})^2. \quad (4)$$

For more details about dynamic programming and run-length coding approach, please refer to [25]. At this point, for each cell  $c_i \in C$ , an array  $\Lambda_i = [\lambda'_1, \dots, \lambda'_n]$  (with  $n_i=6$  for regular shapes) can be defined, where each  $\lambda'_j$  indicates the best compression factor for cell  $c_i$  associated to  $RD_{d_j}$  on direction  $d_j \in S_{ho}$  and  $1 \leq \lambda'_j \leq ||RD_{d_j}||$ . For each  $\lambda'_j$ , a partition vector  $M_j = [\mu'_{j1}, \dots, \mu'_{j\lambda'_j}]$  represents the compressed sequence, for the  $j$ -th side of cell  $c_i$ ; each element  $\mu'_{j_k}$  has an associated partition value  $p^{\mu'_{j_k}}$ , belonging to the  $j$ -th Partition Set  $PS_j^i$ , defined as:

$$p^{\mu'_{j_k}} = \begin{cases} [d_j - \frac{\pi}{6}, \mu'_{j_k} + \frac{(\mu'_{j_{k+1}} - \mu'_{j_k})}{2}] & k=1 \\ [\mu'_{j_k} - \frac{(\mu'_{j_k} - \mu'_{j_{k-1}})}{2}, \mu'_{j_k} + \frac{(\mu'_{j_{k+1}} - \mu'_{j_k})}{2}] & 1 < k < \lambda'_j \\ [\mu'_{j_k} - \frac{(\mu'_{j_k} - \mu'_{j_{k-1}})}{2}, d_j - \frac{\pi}{6}] & k = \lambda'_j \end{cases} \quad (5)$$

In the next subparagraph the way  $M^i = [M^i_1, \dots, M^i_n]$  and

$PS^t = [PS^t_1, \dots, PS^t_{n_t}]$  are used will be described in depth, in order to give a detailed dissertation on how the Markovian theory is introduced to make predictions. It must be observed that each  $\lambda^t_j$  has to be determined accurately: the minimum value is 1 (maximum compression, as in our previous works), while the maximum is  $J$  (no compression, but the number of possible directions is the same as the number of roads on side  $j$ ). In the performance section, an in detailed analysis is introduced in order to choose the right value of  $\lambda^t_j$  for each side.

### B. Markovian modeling based on roads compression

In this subparagraph, the Markovian prediction theory is introduced and the related model is proposed. Figure 4 resumes the different steps explained before referring to a generic cell  $c_t$ , with which a set of roads has been associated to each side of the coverage cell and then used to carry on a dynamic compression (1); then a partitioned set of possible "virtual roads" directions has been obtained (2); the last step is the definition of a Markovian prediction model and the association of the partitioned ranges  $p_{\mu_{jk}}$  to the states of the model (3).

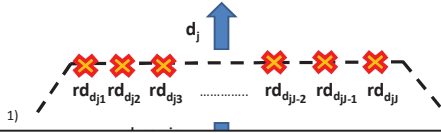


Fig. 4. Roads-to-states process illustration.

The considered model is an extension of the FSMC previously proposed [3], [15], [17]. In fact, given the vectors  $M^t$  and  $PS^t$  defined in the previous section, with  $\|PS^t\| = \|M^t\| = n_t$ , the idea is to associate one state of the Markovian model to each partition subset, representing a compressed set of roads, for each side of  $c_t$ . So, with this aim, remembering that:

$$M^t = \left\{ \begin{array}{l} [\mu^t_{11}, \mu^t_{12}, \dots, \mu^t_{1\lambda_1}] \\ [\mu^t_{21}, \mu^t_{22}, \dots, \mu^t_{2\lambda_2}] \\ \dots \\ [\mu^t_{n_1}, \mu^t_{n_2}, \dots, \mu^t_{n\lambda_n}] \end{array} \right\} \quad PS^t = \left\{ \begin{array}{l} [p^t_{\mu_{11}}, p^t_{\mu_{12}}, \dots, p^t_{\mu_{1\lambda_1}}] \\ [p^t_{\mu_{21}}, p^t_{\mu_{22}}, \dots, p^t_{\mu_{2\lambda_2}}] \\ \dots \\ [p^t_{\mu_{n_1}}, p^t_{\mu_{n_2}}, \dots, p^t_{\mu_{n\lambda_n}}] \end{array} \right\} \quad (6)$$

a Markov chain with the structure of fig. 5 can be associated to a cell  $c_t$ . For the sake of simplicity and readability we did not depict a two-dimensional Markov chain and, in fig. 5, the connections between the chains associated to different sides resume all the possible transitions among two generic states  $s_{j_1k_1}$  and  $s_{j_2k_2}$ , with  $j_1 \neq j_2$ . A road  $rd_{d_{j_1}}$ , that intercepts cell  $c_t$  on side  $j$ , is said to belong to state  $s_{jk}$  if:

$$rd_{d_{j_1}} \in p^t_{\mu_{jk}}. \quad (7)$$

The proposed Markovian road-compression model, illustrated in fig. 5, associates one state of the chain to one subset of a coverage side.

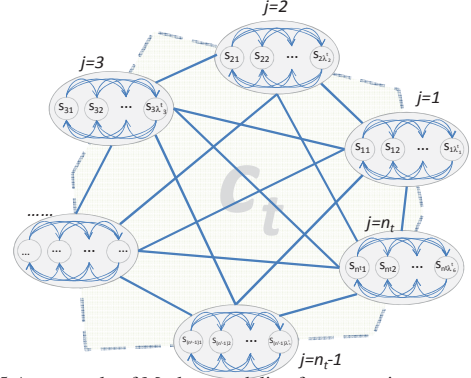


Fig. 5. An example of Markov modeling for a generic coverage shape.

The set of possible states for cell  $c_t \in C$  is  $\Omega^t = \{s_{11}, \dots, s_{1\lambda_1}, s_{21}, \dots, s_{2\lambda_2}, \dots, s_{n_1}, \dots, s_{n\lambda_n}\}$  and the finite state sequence is  $Q = q_1, q_2, \dots, q_m$ , with:

$$\|\Omega^t\| = \sum_{j=1}^{n_t} \lambda^t_j \quad \text{and} \quad \|Q\| = m, \quad (8)$$

where  $m$  is the length of the observation sequence. For cell  $c_t \in C$ , as known from theory, three key elements can be defined for its Markov chain  $MC^t$ : a set of state transition probabilities  $\Pi^t$ , the initial probability array  $\sigma^t$  and the state sojourn times array  $ST^t$ :

$$\Pi^t = \{\pi^t_{j_1k_1-j_2k_2}\}, \pi^t_{j_1k_1-j_2k_2} = p(q_{l+1} = s_{j_2k_2} / q_l = s_{j_1k_1}) \quad (9)$$

where  $q_l$  represents the current state and  $\pi^t_{j_1k_1-j_2k_2} \geq 0, 1 \leq j \leq n$ ;

$$\sigma^t = \{\sigma^t_{jk}\}, \sigma^t_{jk} = P(q_1 = s_{jk}), \quad 1 \leq j \leq n \quad (10)$$

$$ST^t = \{\varepsilon^t_{jk} / P(\varepsilon^t_{jk} < \bar{\varepsilon}) = \int_{-\infty}^{\bar{\varepsilon}} f^t_{jk}(x) dx, \quad 1 \leq j \leq n\} \quad (11)$$

where  $f^t_{jk}(x) = pdf^t_{jk}$  is the probability density function (pdf) associated to state  $s_{jk}$  sojourn time. We can write that the  $MC^t$  can be completely described as follows by a triplet:

$$MC^t = (\Pi^t, \sigma^t, ST^t) \quad (12)$$

Figure 6 illustrates an example of how a distributed set of  $MC^t$   $MC = \{MC^t, 1 \leq t \leq c\}$  can be used to model the whole cellular system (in the general case of irregular shapes).

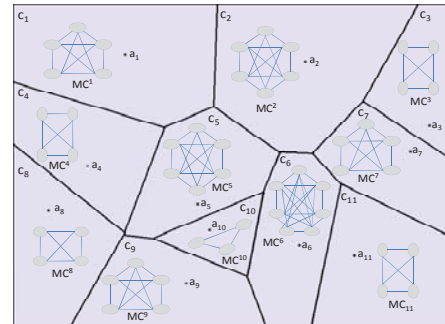


Fig. 6. Wireless cellular system modeling through MCs (c=11).

Supervised training can be approached because the observations of MHs movements are available (in our case by a detailed system simulator, as explained in next sections), so  $MC^t$  inputs and desired outputs are known. Training

observations consist in a set of hand-over direction sequences. The Maximum Likelihood Estimation (MLE) can be used for evaluating of  $\mathbf{IT}$ ,  $\mathbf{\sigma}$ ,  $\mathbf{ST}$  as follows:

$$\pi^t_{j_1k_1-j_2k_2} = \frac{TR^t(s_{j_1k_1}, s_{j_2k_2})}{N^t(s_{j_1k_1})} \quad (13), \quad \sigma^t_{jk} = \frac{FIRST^t(q_1 = s_{jk})}{N^t(q_1)} \quad (14)$$

$$pdf^t_{jk} = pdf_{CST^t} \quad (15)$$

where  $1 \leq j \leq n_t$ ,  $1 \leq t \leq c$ ,  $TR^t(s_{j_1k_1}, s_{j_2k_2})$  is the number of observed transitions from state  $s_{j_1k_1}$  to state  $s_{j_2k_2}$  in cell  $c_t$  (a transition from  $s_{j_1k_1}$  to  $s_{j_2k_2}$  occurs when, in the training data, a MH hands-in cell  $c_t$  from side  $j_1$  on a road  $rd_{dj_1}$  belonging to compressed partition  $p^t_{\mu_{j_1}}$  and hands-out to side  $j_2$  on a road  $rd_{dj_2}$  belonging to compressed partition  $p^t_{\mu_{j_2}}$ ),  $N^t(s_{j_1k_1})$  is the number of transitions from state  $s_{j_1k_1}$  to any other state of  $c_t$ ,  $\sigma^t_{jk}$  represents the probability that state  $s_{jk}$  is the first observed state ( $q_1$ ) in the training observations for  $c^t$  and it is calculated as the ratio between the number of occurrences of  $s_{jk}$  being the first observed state  $FIRST^t(q_1=s_{jk})$  and the number of total observations of first states  $N^t(q_1)$ . For the state sojourn times array  $\mathbf{ST}^t$ , it must be noticed that, in the proposed model, the time elapsed from the hand-in to the hand-out in a given cell  $c_t$  matches with the CST of the same cell, independently of the involved sides/partitions (as demonstrated in [3], [15], [24]). From previous research results, we can state that the pdf of  $CST^t$  follows a Gaussian distribution, so the related parameters can be evaluated through simulation campaigns (as shown later). Details about learning and evaluation of the model can be found in [27], [28]. It is clear that, before the prediction algorithm takes place, each  $MC^t$  belonging to cell  $c_t \in C$  needs to be trained, so the terms expressed in equations (13, 14, 15) can be evaluated by observing MHs movements (in our case we carried out a campaign of simulations, observing MH behaviors from the traces generated by [4]).

### C. MultipleXing (MUX) of passive reservations

Once the most probable cells are predicted, the signalling protocol should be able to enhance resources utilization through the employment of a resource multiplexing scheme: the idea is to make the earlier-reserved bandwidth in  $c_t$  for an MH available for other users before the MH arrives in  $c_t$ , so it can be considered as an available resource when other incoming traffic makes a service request to  $c_t$ . In addition, another reason for employing system multiplexing is represented by the enhancement of prediction error: although an MH fails to find a pre-reserved bandwidth on a new access point (i.e. it has arrived in a not-predicted cell) the availability of more resources reduces the probability of dropping the flow. Recalling briefly that shown in previous works [3], [15], the pdf of average time spent by a user in a coverage cell  $c_t \in C$  can be well approached by a Gaussian distribution  $N^t(mean^t_{CST}, stdev^t_{CST})$  and its parameters can be evaluated by observing real samples of MHs movements. Given  $\tau^t_{in}(\alpha)$  and  $\tau^t_{out}(\alpha)$ , which represent the predicted hand-in and hand-out times to/from a cell respectively for the  $\alpha$ -th hand-off event in cell  $c^t$ , then:

$$\tau^t_{in}(\alpha+1) = \tau^t_{out}(\alpha) + \bar{\tau}^t(\alpha), \quad (16)$$

where  $t_l \neq t$  is the identifier of the cell to which a MH will hand-in from  $c^t$  at the  $(\alpha+1)$ -th hand-over event, and  $\bar{\tau}^t$  is a

realization of  $N^t(mean^t_{CST}, stdev^t_{CST})$ , which can be obtained with the Box-Muller algorithm [29], [30]:

$$\bar{\tau}^t = stdev^t_{CST} \cdot \sqrt{-2 \ln u_1} \sin(2\pi u_2) + mean^t_{CST} \quad (17)$$

where  $u_1$  and  $u_2$  are two random numbers, uniformly distributed in  $(0,1]$ . If eq.(16) is generalized, then:

$$\tau^t_{in}(\alpha+1) = \tau^t_{in}(\alpha) + \sum_{m=0}^{\alpha} [\bar{\tau}^t(m)] \quad (18)$$

where  $t_m$  is the predicted cell identifier for the  $m$ -th hand-off and  $\tau^t_{in}(0)$  is assumed to be the time at which the call has originated in cell  $c_{t_0}$ . So, for a generic  $\alpha$ -th hand-over event, the time at which a MH will enter a cell can be evaluated by considering statistical distributions. Each coverage cell  $c_t \in C$ , at a certain time, has  $ns^t_a$  slots (or channels) used to accommodate active reservations (incoming calls),  $ns^t_p$  slots used to accommodate passive reservations (in-advance requests) and  $ns^t_f$  free slots. The sum  $ns^t = ns^t_a + ns^t_p + ns^t_f$  represents the total capacity of the cell (initially  $ns^t = ns^t_f$ ) [3], [20], [24]. As illustrated previously, each passive request, indicated with  $req_x$ , has predicted hand-in and hand-out times, as derived in eq. (16), indicated with  $\tau^{t-x}_{in}(\alpha)$  and  $\tau^{t-x}_{out}(\alpha)$  respectively, where  $\alpha$  indicates that the bandwidth reservation of duration  $\tau^{t-x}_{out}(\alpha) - \tau^{t-x}_{in}(\alpha)$  is made for the  $\alpha$ -th hand-off of the  $x$ -th request. If the Time Set ( $TS$ ) of the  $x$ -th request in cell  $c_t$  is defined as:

$$TS^t_x(\alpha) = [\tau^{t-x}_{in}(\alpha), \tau^{t-x}_{out}(\alpha)], \quad \|TS^t_x(\alpha)\| = \bar{\tau}^{t-x}(\alpha) \quad (19)$$

then, two generic passive requests  $x$  and  $y$  have no time intersection if:

$$INTERSECT(x, y) = TS^t_x(\alpha) \cap TS^t_y(\beta) = \emptyset \quad (20)$$

or, equivalently:

$$[\tau^{t-x}_{out}(\alpha) < \tau^{t-y}_{in}(\beta)] \vee [\tau^{t-x}_{in}(\alpha) > \tau^{t-y}_{out}(\beta)] \quad (21)$$

where  $\alpha$ ,  $\beta$  are the hand-off indexes for  $x$ -th and  $y$ -th passive requests respectively. So, fixing the resource slot (bandwidth amount or channel) and assuming that condition of eq. 20 is satisfied among a new incoming passive request and all the existing ones, then the new request can be accommodated in the slot that has been already used.

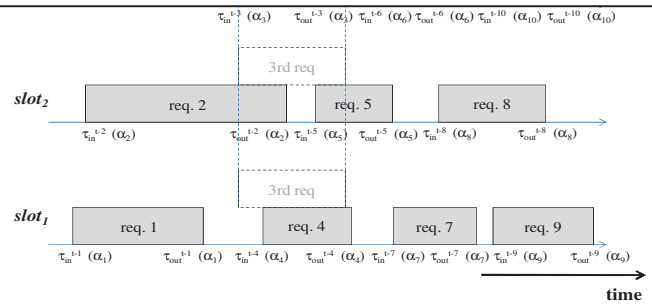


Fig. 7. Typical passive bandwidth management with time multiplexing.

In fig. 7, three slots are considered and the condition of null intersection is verified for requests 1,4,7,9 on slot 1, requests 2, 5, and 8 on slot 2 and requests 3, 6, and 10 on slot 3. The 3-rd request cannot be inserted either in slot 1, because  $INTERSECT(3,4) \neq \emptyset$ , or in slot 2, because

$INTERSECT(3,2) \neq \emptyset$  and  $INTERSECT(3,5) \neq \emptyset$ . So, when a slot cannot be used for an incoming request, a new “free” slot, if it exists, has to be chosen and a criterion should be followed. Since the available slots represent a scarce resource, the fairness criterion should be respected among the new arriving requests. Therefore, an appropriate allocation policy must be employed, so we considered the following index [31] for the whole cell  $c_t$ :

$$fair_{c_t} = \frac{1}{ns^t} \cdot \left[ \sum_{j=1}^{ns^t} util(slot_j^t) \right]^2 / \sum_{j=1}^{ns^t} util^2(slot_j^t) \quad (22)$$

where:

$$util(slot_j^t) = \sum_k [\tau_{out}^{t-k}(\alpha_k)_j - \tau_{in}^{t-k}(\alpha_k)_j]. \quad (23)$$

Equation 22 gives an idea of the equality of the allocation of the slots of each cell: if all the slots of  $c_t$  get the same amount of passive requests, then it goes to 1; when the assignment is unfair, it goes to 0. A threshold value  $thr_{fair}$  is considered (the same for each  $c_t$ , without loss of generality): cell  $c_t$  respects the fairness condition if  $fair_{c_t} \geq thr_{fair}$ .

#### D. Prediction and Multiplexing Integration: DPBMA

Before the prediction algorithm takes place, each  $MC^t$  belonging to cell  $c_t \in C$  needs to be trained, so the terms expressed in equations 13, 14, and 15 can be evaluated by observing MHs movements (in our case we carried out a campaign of simulations, observing MH behaviors from the traces generated by [4]). In this way, for each cell  $c_t \in C$  the related  $MC^t$  model is completely characterized. The integration follows the diagram illustrated in fig. 8.

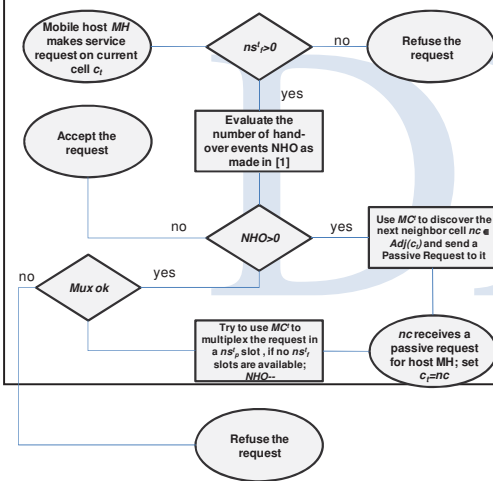


Fig. 8. Flow Diagram of reservation protocol integrated with the predictor.

The protocol starts with the active service request performed by MH on cell  $c_t$ ; if there are not free slots in  $c_t$ , the call is refused, otherwise cell  $c_t$  applies the results obtained in [3], [24] to evaluate the number of predicted hand-over events  $NHO$ . If no hand-over events are predicted, then the call is accepted (the MH will visit only the current cell  $c_t$ ), otherwise, the  $MC^t$  is evaluated and a passive bandwidth request is sent to the predicted neighbor cell  $nc \in Adj(c_t)$ , also containing the number of remaining hand-over events  $NHO-1$ . The cell  $nc$  becomes the current one and it tries to apply the multiplexing algorithm of  $MC^t$  introduced in the previous sub-section; if there is no space for the passive request, a negative message is

sent to MH, if  $NHO > 0$  the last two steps are repeated, and ( $NHO = 0$ ) the passive request is accepted. Following the same approach of [3], when a new passive request arrives in cell  $c_t$ , the proposed algorithm tries to obtain  $util(slot_j^t) \equiv util(slot_k^t)$ , satisfying the criterion of eq. 22, so:

- 1) When a new passive request  $req_x$  arrives to the cell  $c_t$  and fairness criterion is not satisfied, candidate  $ns^t_p$  slots are sorted in increasing order of  $fair_{c_t}$ ; set  $j=1$ ;
- 2) Starting from the  $j$ -th element of the ordered list, if the condition of eq. 20 (or eq. 21) is satisfied for each existing passive reservation, then  $req_x$  can be accommodated in the  $j$ -th slot  $ns^t_j$ ; otherwise  $j=j+1$  and step 2 is fully repeated;
- 3) If also the last slot is full, then  $req_x$  will be not accepted,  $c_t$  sends a negative message to the mobile host.

#### E. Complexity

From a computational point of view, different phases should be considered:

- **LOCALIZATION COMPLEXITY (LC)**: as already stated, before making mobility predictions, or collecting MHs directional statistics, all coverage cells have to define the  $RD_{dj}$  sets for each side, with  $j=1, \dots, n_t$ . For this objective, the determination of DoA (or location) for MHs implies a certain complexity  $O(LOC)$ , depending on the considered physical parameters. In this way, all the cells of the considered network can obtain a complete set of roads, in the worst case, with a complexity of:

$$LC = MHN \cdot O(LOC) \quad (24)$$

where MHN is the number of observed mobile hosts; because it must be applied for all the  $n$  directions for each observed MH; it must be noticed that the localization algorithm needs to be executed only once, during the training phase and not for predicting movements;

- **COMPRESSION COMPLEXITY (CC)**: at this point, once the number of roads has been determined, each cell can apply the compression algorithm, in order to optimize the number of states of the associated Markov chain. From [25], it is known that the complexity for a generic numeric data compression is  $O(Z^2 \log Z)$ , when the optimal  $\lambda_j$  has to be determined ( $Z$  is the length of the numeric sequence to be compressed). For a cell  $c_t \in C$ , it can be written that:

$$CC = n_t \cdot O(RD_{MAX}^2 \log RD_{MAX}) \quad (25)$$

applied for the  $n_t$  sides of  $c_t$ , where  $RD_{MAX}$  is:

$$RD_{MAX} = \max_j \{ \| RD_{dj} \| \} \quad (26)$$

Since the compression level is strictly related to the prediction error (as shown in section IV), in our proposal the determination of the optimum value of  $\lambda_j$  is not considered. We analyzed, instead, how  $CC$  varies in function of  $J$  (number of roads on side  $j$  to be compressed) and  $\lambda_j$ , because we are interested in finding a good trade-off in terms of complexity and prediction error. In particular, in fig. 9, the trend of  $CC$  (for a generic cell  $c_t$  and a generic side  $j$ ) is depicted. In order to make the values comparable for different cases, they have been normalized in  $[0,1]$  by dividing each obtained value by the maximum one. The curves were obtained by fixing  $J$  and considering the computational complexity for different values of  $\lambda_j$ , while determining each possible cut-set of the original binary tree.

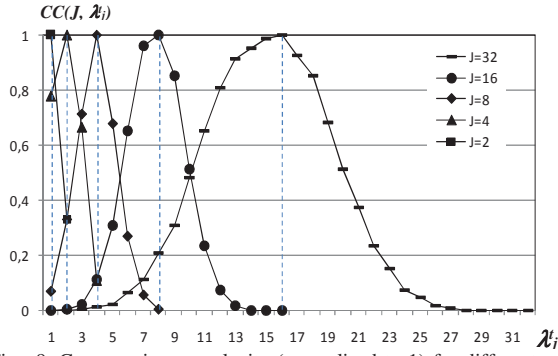


Fig. 9. Compression complexity (normalized to 1) for different number of roads ( $J$ ) and different values of desired  $\lambda_j$ .

As illustrated in [25], when dealing with tree cut-set determination, the complexity goes increasing until  $\lambda_j$  is equal to  $J/2$  (because an increasing number of combinations is needed), so the worst case is obtained for a number of compressed roads equal to  $J/2$ . Lower values ( $\lambda_j < J/2$ , higher compression) or higher values ( $\lambda_j > J/2$ , lower compression) lead the system to a more acceptable complexity. Also in this case, this operation is executed once, after the number of roads has been determined;

- **TUNING COMPLEXITY (TC)**: after the compression phase, for each cell the number of partitioned ranges for each side has been determined, so the number of states is also known. In particular, the number of states for chain  $MC^i$  associated to  $c_i$ , indicated with  $\|MC^i\|$ , is given by:

$$\|MC^i\| = \sum_{j=1}^{\lambda_j} \lambda_j^j \quad (27)$$

In this phase, the terms of eq. 13, 14, and 15 need to be obtained; the algorithm, simply evaluates the values of the parameters of those equations, by observing users mobility, determining their DOA, recognizing the membership to the partitioned sets (ranges expressed in eq. 6) and updating the parameters, so the complexity becomes:

$$TC = \|MC^i\| \cdot O(LOC) \quad (28)$$

At this point, it must be outlined that, for each  $c_i \in C$ , the total complexity given by  $C_{TOT} = LC + CC + TC$  is considered only once in the training period (all the chains learn the roads topology and users mobility behaviour). Once the parameters of the model associated to  $c_i \in C$  are defined, the prediction is made in a constant time, using the transition matrix and the CST information.

#### IV. PERFORMANCE EVALUATION

In order to evaluate the proposed integration in terms of average prediction error, system utilization, CDP and CBP, we considered real mobile environments: Citymob mobility generator and the C4R GUI [4] were considered, as they give the opportunity to obtain mobility traces from real maps. In particular, we used many urban maps of some European cities (about 2.5 Km<sup>2</sup> for each scenario), over which a set of coverage cells was considered. For regular shapes, all the cells are supposed to have the same radius  $R$  ( $r_i = R, \forall c_i \in C$ ) and  $R \in [10, 1000]$  meters; for irregular shapes, Voronoi tessellations were considered, as illustrated later. Regarding the regular

coverage ranges, we can suppose that for  $R \in [10m, 30m]$  the IEEE802.11ac, ad or HetNet femto-cells [28] technologies are used, for  $R \in [100m, 1000m]$  the system can be covered by 3G cells and for  $R \in [800m, 1000m]$  the access technology can belong to 4G. We did not consider 1/2G to avoid analyzing old technologies.

#### A. Algorithm modeling and parameters description

As stated before, different cities were considered and, for all of them, obtained results are comparable: without loss of generality, we show the obtained curves for the city of London. We considered a variable coverage range for the regular case. Figure 10 illustrates, on the left, the obtained regular coverage for  $R=140m$  and  $GR_i \cong GR_j \cong 1600m$  (in this case  $c=42$ ), and on the right, a Voronoi diagram with  $c=33$ .

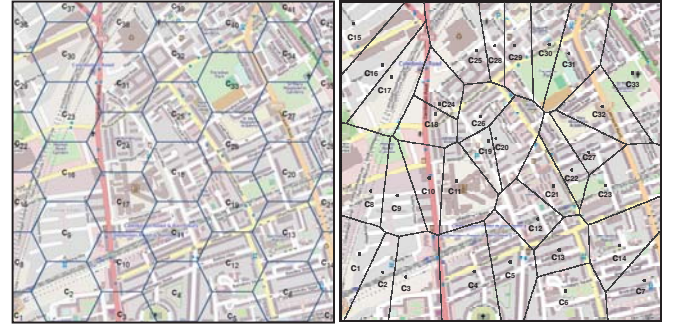


Fig. 10. The set of 42 (regular) and 33 (irregular) cells used to cover GR.

Once the GR topology and the map have been determined, the compression algorithm needs to be executed for all cells (with a total computational complexity of  $c \cdot CC$ ).

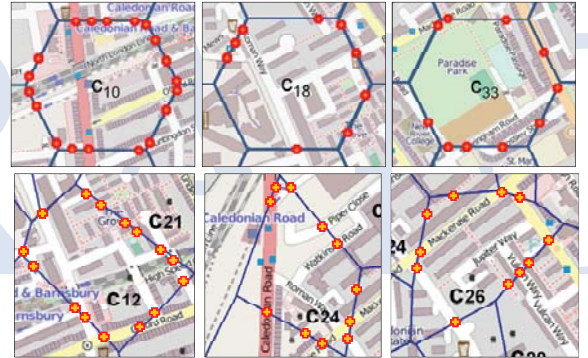


Fig. 11. Road sets for some cells of the considered network.

In order to choose the right number of partitions for each  $c_i$  and for each related direction, a compression factor  $cf_i$  is chosen, so:

$$\lambda_j = \begin{cases} 0 & \text{if } \|RD_{dj}\| = 0 \\ 2^{\lceil \log_2[(1-cf_i) \cdot \|RD_{dj}\|] \rceil} & \text{if } \|RD_{dj}\| \neq 0 \text{ and } (1-cf_i) \cdot \|RD_{dj}\| > 1 \\ 1 & \text{else} \end{cases} \quad (29)$$

where the  $\lceil \cdot \rceil$  operator indicates the integer part. For each cell  $c_i$ , a number of total slots  $ns^i$  equals to 20 was considered and each reservation occupies a single slot in each cell (active or passive). Only for example, Table III resumes the values of  $\|RD_{dj}\|$  and  $\lambda_j$  for three regular cells ( $c_{10}$ ,  $c_{18}$ ,  $c_{33}$ ) and three irregular cells ( $c_{12}$ ,  $c_{24}$ ,  $c_{26}$ ) as illustrated in fig. 11.

TABLE III.  
NUMBER OF ROADS FOR EACH DIRECTION FOR CELLS  $C_{10}$ ,  $C_{18}$ ,  $C_{33}$  (REGULAR)  
AND  $C_{12}$ ,  $C_{24}$ ,  $C_{26}$  (IRREGULAR).

$c_i$	$d_1$	$d_2$	$d_3$	$d_4$	$d_5$	$d_6$	$d_7$	$d_8$	
10	4	4	2	3	3	3	-	-	RD <sub>di</sub>    <sub>10</sub>
12	6	3	4	1	1	-	-	-	RD <sub>di</sub>    <sub>12</sub>
18	2	1	3	0	1	2	-	-	RD <sub>di</sub>    <sub>18</sub>
24	3	3	3	2	-	-	-	-	RD <sub>di</sub>    <sub>24</sub>
26	2	0	4	1	0	0	3	1	RD <sub>di</sub>    <sub>26</sub>
33	1	2	1	1	3	2	-	-	RD <sub>di</sub>    <sub>33</sub>

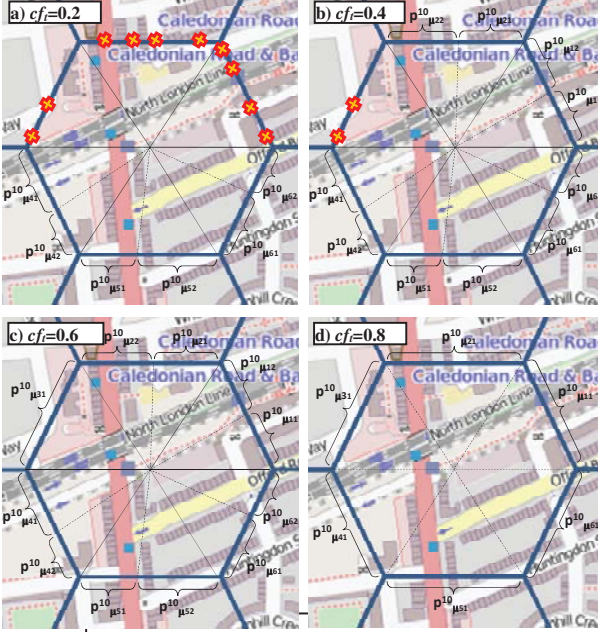


Fig. 12. Road sets partitioning for cell  $c_{10}$  with different  $cf$  values.

Regarding fig. 12, basing the dissertation on the first row of table IV, we can observe that for high values of  $cf_i$ , a lower number of virtual roads (i.e. number of states for the model) is obtained for each direction, with a lower granularity. Table IV indicates the obtained  $\Lambda_i$  sets for different values of  $cf_i$ . Considering the cases of  $cf_i=0.2$  and  $cf_i=0.8$ , the Markovian models for cell  $c_{10}$  become the ones of fig. 13.

TABLE IV.

THE NUMBER OF COMPRESSED ROADS SET FOR THE CONSIDERED CELLS.

$c_i$	$cf_i=0,2$	$cf_i=0,4$	$cf_i=0,6$	$cf_i=0,8$	
10	{4,4,2,2,2,2}	{2,2,2,2,2,2}	{2,2,1,2,2,2}	{1,1,1,1,1,1}	$\Lambda_{10}$
12	{4,4,4,1,1}	{4,2,4,1,1}	{2,2,2,1,1}	{1,1,1,1,1,1}	$\Lambda_{12}$
18	{2,1,1,0,1,2}	{2,1,2,0,1,2}	{1,1,2,0,1,1}	{1,1,1,0,1,1}	$\Lambda_{18}$
24	{2,4,4,2}	{4,2,4,2}	{2,2,2,1}	{1,1,1,1}	$\Lambda_{24}$
26	{2,0,2,1,0,4,1}	{2,0,2,1,0,0,2,1}	{2,0,1,1,0,0,1,1}	{1,0,1,1,0,0,1,1}	$\Lambda_{26}$
33	{1,2,1,1,2,2}	{1,2,1,1,2,2}	{1,1,1,1,2,1}	{1,1,1,1,1,1}	$\Lambda_{33}$

In particular for  $cf_i=0.2$  (low compression),  $\Lambda_{10}=\{4,4,2,2,2,2\}$  (starting from an initial condition of  $\{4,4,2,3,3,3\}$  for  $cf_i=0$ : directions  $d_1$ ,  $d_2$  and  $d_3$  are not affected by compression, so the original roads are still considered). The extreme case is  $cf_i=0.8$ , for which  $\Lambda_{10}=\{1,1,1,1,1,1\}$ . The same trend was obtained for all the other cells. In order to understand better how the different road sets are partitioned, cell  $c_{10}$  has been considered graphically, fig. 13, for different compression factor values (0.2, 0.4, 0.6 and 0.8).

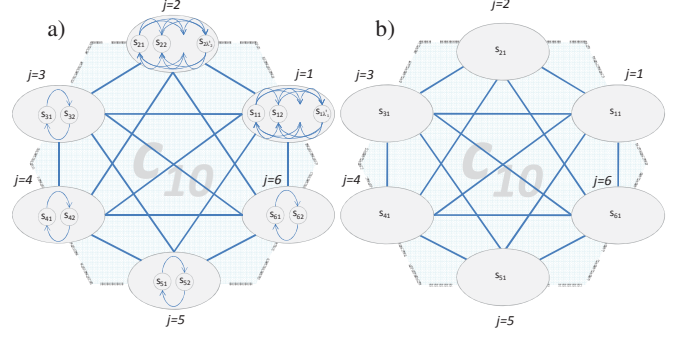


Fig. 13. Markov chain for  $c_{10}$  with a)  $cf_i=0.2$  (16 st.) and b)  $cf_i=0.8$  (6 st.).

## B. Obtained results

First of all, a training campaign was performed in order to obtain the elements of  $MC^t$  and  $CST^t$ , relating to the considered map. We considered the Kraub mobility model [4] (with Acceleration =  $1.4m/s^2$ , Deceleration  $2m/s^2$ ,  $\sigma=0.5$  and  $\tau=0.2s$ ) for 400 simulations with 1200s of duration and a number of 300 vehicles for each run. Mobility log-files were obtained and, then, the coverage set of cells was considered (regular and irregular). Different compression factor  $cf_i$  values were used for regular and irregular coverage, as well as different coverage radius  $R$  values for the regular one. So, once the road topology and the number of states were determined for each cell, then a set of dedicated and supervised training campaigns was carried out, based on mobility log files, with the aim of evaluating the terms expressed in equations 13, 14 and 15 (the Maximum Likelihood Estimation - MLE method has been used). Figure 14 gives an idea of the obtained parameters, for regular coverage and  $R=110m$ .

$\Pi^{10}$	$s^{10}_{11}$	$s^{10}_{12}$	$s^{10}_{21}$	$s^{10}_{22}$	$s^{10}_{31}$	$s^{10}_{32}$	$s^{10}_{41}$	$s^{10}_{42}$	$s^{10}_{51}$	$s^{10}_{52}$	$s^{10}_{61}$	
$s^{10}_{11}$	0.08721	0	0	0.21378	0	0	0.23244	0.08734	0	0.22354	0	0.15665
$s^{10}_{12}$	0.03945	0	0.08922	0.26443	0.10143	0	0.14333	0.09112	0.27882	0	0	0
$s^{10}_{21}$	0.00000	0.04333	0.56445	0.34004	0	0.05164	0	0	0	0	0	0
$s^{10}_{22}$	0.05443	0.01134	0.31830	0.33703	0	0	0	0	0.28445	0	0	0
$s^{10}_{31}$	0.01557	0	0	0	0.98022	0	0	0	0	0	0	0
$s^{10}_{32}$	0	0	0	0	0.58111	0.41998	0	0	0	0	0	0
$s^{10}_{41}$	0.35378	0.27983	0	0	0	0	0.19881	0	0	0	0	0
$s^{10}_{42}$	0.04457	0.01212	0	0	0	0	0	0.64773	0.29711	0	0	0
$s^{10}_{51}$	0	0.40876	0	0.12344	0	0	0.11222	0.15884	0.19772	0	0	0
$s^{10}_{52}$	0	0	0	0	0	0	0	0	0	0.15777	0.84333	0
$s^{10}_{61}$	0	0	0	0	0	0	0	0	0	0.65488	0.34552	0
$s^{10}_{62}$	0.14333	0	0	0	0	0	0	0	0	0	0	0.85552

$$\sigma^{10} = [.253, .278, .056, .045, .251, .033, .001, .042, .002, .001, .021, .021]$$

Fig. 14. Transition probability matrix  $\Pi^{10}$  for  $c_{10}$ , with  $cf_{10}=0.4$  and the probabilities of first states  $\sigma^{10}$ .

We considered a Call Arrival Rate (CAR) of 5 reqs/s. Due to space limitations, only the parameters of one cell are depicted, in particular for cell  $c_{10}$ . Figure 14 illustrates the transition probability matrix  $\Pi^{10}$ , for which each element is evaluated as the mean value on all the carried-out simulations. The initial probabilities vector for cell  $c_{10}$  is also shown. Mobility effects on the borders are ignored by neglecting mobile trajectories that go outside the coverage set. Figure 15 shows how the system responds to DPBMA in terms of system utilization for a regular coverage scenario; it is calculated as:

$$u_{\%} = \frac{1}{c} \cdot \sum_{t=1}^c \frac{ns'_t}{ns^t} \quad (30)$$

that is to say, the average of the ratio between the active bandwidth slots and the total ones, for each cell.

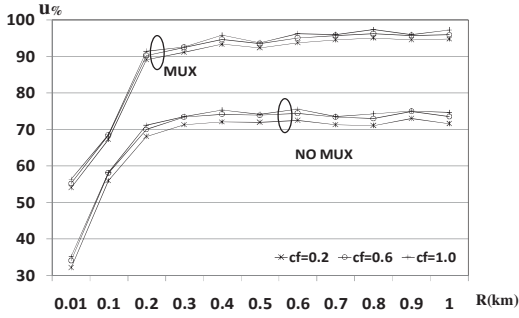


Fig. 15. Average system utilization for different values of  $R$  (regular coverage) and compression factors  $cf$ .

It is evident how, without the multiplexing approach (NO MUX), the system is under-utilized ( $u\%$  belongs to the range [31, 72]). There is an increasing trend for higher coverage radius: when the number of cells decreases (from  $\approx 7900$  to  $\approx 3$ ), there is a lower number of passive reservations (lower cells have to be predicted because of the higher geographical covered region); in this case, also the protocol overhead decreases, because there is a lower number of cells among which the signalling packets have to be exchanged. Regarding the compression factor  $cf$ , it can be noticed how it does not affect the performance in terms of utilization: the maximum gap is about 2.2%. On the contrary, more acceptable results are obtained when the multiplexing scheme (MUX) of DPBMA is activated, giving the possibility of re-using passive slots. It is evident how the introduction of multiplexing of bandwidth gives the possibility of achieving a higher utilization to the system, since passive resources are re-used, taking into account the time of arrival of mobile hosts. It is shown how a gain of about 13%-25% is obtained, depending on coverage radius and compression factor. The increasing trends are similar to the ones explained before. In fig. 16, the obtained average utilization for the irregular coverage map is shown.

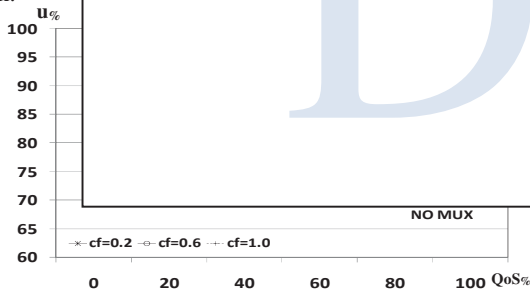


Fig. 16. Average system utilization for different values of QoS requests percentage and compression factor  $cf$  (irregular coverage).

The values on the x-axis represent the percentage of service requests requiring passive reservations; the other ones are served by simply reserving bandwidth in the current cell (only active reservations). It can be seen how, also in this case, the compression factor  $cf$  does not affect the obtained curves, while there is a different trend for MUX and NO MUX scenario. When the passive requests are not multiplexed, the huge amount of passive bandwidth is not used by flows, until

the respective MH arrives into the considered coverage. For this reason, system utilization decreases for higher percentages of QoS requests (more unused passive resources). In the MUX case, instead, although there are passive reservations, resource does not remain unused, so they can be multiplexed until the MH arrives into the cell. In fig. 17, the prediction error evaluated for the first four hand-over events is illustrated. For a single simulation, it is evaluated as the ratio  $m_{NOK}/m_{TOT}$ , where  $m_{NOK}$  is the number of users that do not find a passive reservation after four hand-overs and  $m_{TOT}$  is the number of total users considered during simulation time. The  $cf$  values of 0.2, 0.6 and 1 have been considered, with activated (MUX) or deactivated (NO-MUX) multiplexing scheme. Also in this case, the multiplexing scheme does not heavily affect the trend (the maximum gap is around 2.3%).

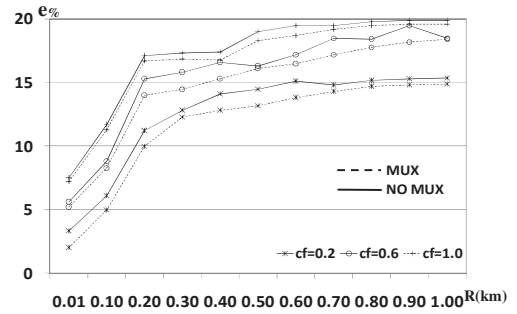


Fig. 17. Average prediction error for different values of  $R$  and compression factor  $cf$ , in MUX and NO-MUX cases (regular coverage).

Even in this case, the trend increases both for higher coverage radius (host movements are more casual if the considered area is larger) and  $cf$  values (system loses granularity about users movements, because less roads are considered, as well as less chain states). Nevertheless, the committed prediction error falls below 20%. In this case, it is assumed that only one cell is considered as the next one for the first hand-over. As shown in our previous works [17], [20], the error can be decreased if more than one cell is considered as future ones for the first hand-over. It has been verified that the maximum value for  $e\%$  is around 9%-10%, considering 2 next cells for each hand-over.

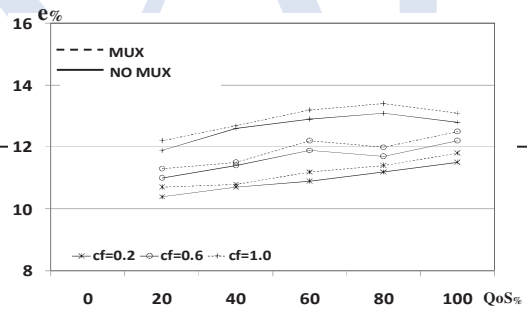


Fig. 18. Average prediction error for different values of QoS requests percentage and compression factor  $cf$  (irregular coverage).

From fig. 18, it is possible to see the trend of the average prediction error for the considered irregular map. Clearly, when the percentage of QoS requests is null, no errors can be obtained. According to the previous case, increasing the  $cf$  leads to a higher prediction error: it belongs to the range [10.1%, 14.2%]; the increasing in function of QoS requests

percentage can be neglected (it is lower than 1.1%). Figure 19 shows the trend of the passive reservations made on cell  $c_{18}$  of the regular coverage network, for slots 1, 10 and 20, with  $R=110m$  and  $cf=0.4$  (obviously the MUX scheme is active). The observation time in the figure is 120s and it is shown how the passive reservations are correctly distributed over the available slots (only the trend of 3 over 20 slots is illustrated, in order to avoid graphical overlays). In the first considered amount of time (from 0 to 50 s) the system is observing a transient period, after which a steady condition is reached. This behaviour was observed for all the cells of the system (with regular or irregular coverage).

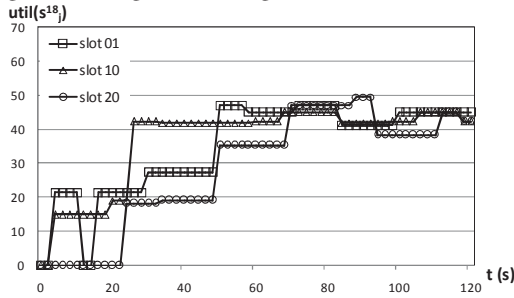


Fig. 19.  $util(s^{18})$  for  $c_{18}$  (slots 1,10,20) over time (regular coverage).

In fig. 20 the course of the CBP (the probability that a new service request is blocked) is illustrated. It is evident how for a larger  $R$  it increases, because each cell will cover a larger geographical area (so it will serve more users), while the number of available slots remains the same. In addition, as expected, the  $cf$  value does not affect the policy (the maximum gap is around 0.022), there is a slight decreasing of CBP because, for higher prediction values, the system overestimates the available resources and admits more users. The difference in employing the multiplexing scheme is more evident for a larger coverage radius, although the maximum gap is obtained for 190-210 meters. Before these values the difference is negligible, while for higher values it is evident how, without the multiplexing algorithm, the system suffers more call blockings, since it is not able to face the higher number of service requests. After  $R=600m$  the CBP values become stable.

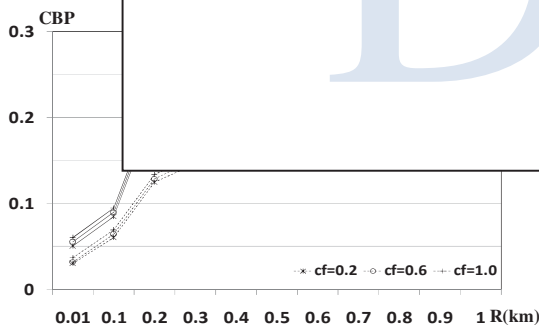


Fig. 20. CBP vs  $R$  and  $cf$  (regular coverage).

Figure 21 confirms the trend for the CBP for the irregular coverage case: it can be observed how it does not depend on the percentage of QoS requests and on the compression factor  $cf$  (maximum gap is around 0.01) but, as in the previous figure, the difference between the MUX and NO MUX cases

is evident. The multiplexing algorithm introduces a decrease in the CBP of about 0.06.

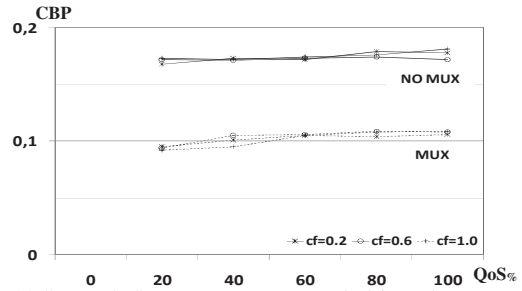


Fig. 21. CBP vs QoS requests percentage and  $cf$  (irregular coverage).

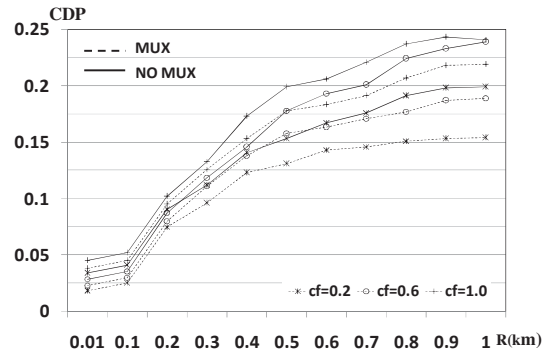


Fig. 22. Trend of CDP vs  $R$  and  $cf$  (regular coverage).

Figure 22 shows the trend of the CDP for different values of  $R$  and  $cf$ . For small coverage areas ( $R < 150m$ ) there is a negligible probability of calls dropping (below 7.5%) because of (based also on the trend of prediction error) more deterministic host movements in the network. In addition, a higher value of  $cf$  causes the prediction algorithm to lose more road information granularity, arriving to the simplest case of one direction for each coverage side: this explains why curves increase their trend for higher  $cf$  values. In this case, the impact of multiplexing is evident. When the system gives the possibility of recycling passive reservations, there will be more bandwidth availability for new incoming calls so, when the prediction algorithm fails to find the right cell, more bandwidth will be available in the cell where the MH has handed-in, giving the possibility to continue the ongoing flow.

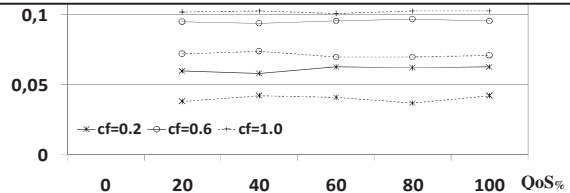


Fig. 23. CDP vs QoS requests percentage and  $cf$  (irregular coverage).

For different  $cf$  values, the larger the coverage area, the higher the CDP reduction, which arrives at about 0.041. Therefore, we can observe that the activation of the MUX algorithm gives the opportunity of reducing the overall average prediction error, since more bandwidth is available

when a prediction fails. Figure 23 shows the trend of CDP for the irregular coverage case: also in this case the multiplexing algorithm gives a contribution to the trend (about 0.042), which is not affected by the QoS requests percentage. Increasing the compression factor will result in a performance worsening: starting from values equal or below 0.05, the CDP increases until 0.106.

### C. Performance comparison for a real scenario

In this subsection, a real scenario is considered, as illustrated in fig. 24. The GR is delimited by the rectangle and the irregular coverage is represented as a Voronoi tessellation. As previously mentioned, our attention does not focus on the way the tessellation is obtained, but the aim of this work is also to demonstrate that the proposed idea is suitable for regular coverage, as well as for irregular ones. As shown,  $C=\{c_1, \dots, c_{22}\}$ ,  $c=22$ ,  $GR_x=12.8\text{Km}$ ,  $GR_y=12.6\text{Km}$ .

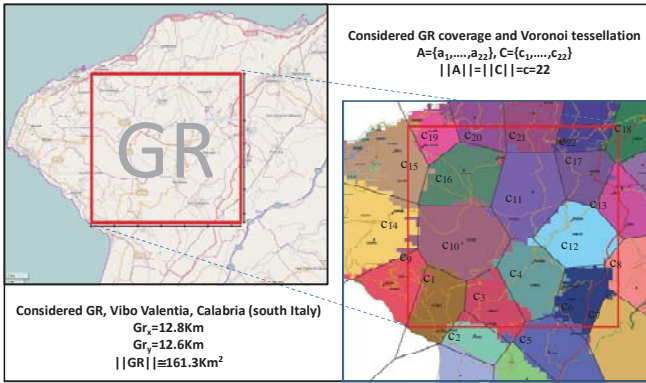


Fig. 24. Real map of the considered GR.

The radio-mobile coverage was obtained by particular telecommunication company measurements, considering UMTS performance of a particular delimited zone in southern Italy (Vibo Valentia province),  $\|GR\|=161.3\text{Km}^2$ . It is shown how the UMTS coverage can be approached by a Voronoi tessellation. Table V summarises the main parameters of the considered cells.

TABLE V.

MAIN RADIO-MOBILE PARAMETERS OF THE CONSIDERED COVERAGE CELLS

CGI	t	CELL	Place	Latitude	Longitude	Irrad. Dir. (°)	Alt. (m)	Tilt (°)
222-01-22511-57310	1	ZC55D2	ROMBIOLO	38 33 54.08	15 56 46.37 E	320	328	0.00
222-01-22511-57005	2	CZ43D1	NICOTERA	38 33 26.15	15 56 19.95 E	98	236	4.00
222-01-22511-57309	3	ZC55D1	ROMBIOLO	38 33 54.08	15 56 46.37 E	60	328	0.00
222-01-21141-56718	4	CZ98D2	CALIMERA	38 33 54.99	16 01 04.03 E	339	276	0.30
222-01-22511-57165	5	ZC19D1	SCIORDELLA	38 31 24.07	16 00 37.38 E	20	75	0.00
222-01-21141-56717	6	CZ98D1	CALIMERA	38 33 54.94	16 01 04.19 E	58	276	2.60
222-01-21141-56630	7	CZ77D2	BIVIO MILETO	38 34 02.67	16 04 03.28 E	146	233	6.00
222-01-21141-56629	8	CZ77D1	BIVIO MILETO	38 34 02.74	16 04 03.41 E	45	233	5.00
222-01-22511-57053	9	CZ55D1	JOPPOLO	38 34 05.26	15 54 11.39 E	10	50	0.00
222-01-21141-57194	10	ZC26D2	ZUNGRI	38 38 08.36	15 57 36.15 E	200	610	1.60
222-01-21141-57193	11	ZC26D1	ZUNGRI	38 38 08.36	15 57 36.28 E	131	610	7.00
222-01-21141-57079	12	CZ61D3	MILETO	38 36 25.77	16 03 47.92 E	300	364	0.70
222-01-21141-57181	13	ZC23D1	IONADI	38 37 51.49	16 03 31.05 E	80	501	2.20
222-01-21141-57278	14	ZC47D2	SPILINGA	38 38 37.08	15 53 32.36 E	150	414	0.00
222-01-21141-64817	15	ZC76D1	BRATTIRO'	38 39 39.25	15 53 58.39 E	60	325	6.00
222-01-21141-57195	16	ZC26D3	ZUNGRI	38 38 08.35	15 57 36.02 E	279	610	4.00
222-01-21141-57183	17	ZC23D3	IONADI	38 37 51.57	16 03 30.96 E	347	501	1.00
222-01-21141-56859	18	CZ06D3	VIBO V.C.	38 40 24.72	16 06 33.90 E	238	561	6.00
222-01-22511-57009	19	ZC44D1	TROPEA BASSA	38 40 22.08	15 52 30.36 E	60	450	0.00
222-01-21141-56982	20	CZ37D2	ZAMBRONE	38 43 04.68	16 00 44.85 E	199	169	0.50
222-01-21141-57142	21	ZC13D2	BRIATICO	38 43 15.61	16 02 14.04 E	178	78	1.00
222-01-21141-64858	22	ZC86D2	VENA	38 39 45.20	16 03 35.74 E	326	484	9.10

We neglect the border effects, considering only the dynamics of GR (inside the square area). In order to evaluate

the effectiveness of the proposed idea, different comparison schemes were considered. As illustrated in the related work section, only a few of them consider multi-step prediction, by taking into account user behavior during the day. In particular, the authors of [9] propose a prediction framework for the User Mobility Profile (UMP). The algorithm does not evaluate the cells that will be traversed by the user but, given its mobility status (position, speed and direction), the probabilities of each cell that the user can cross in a future moment are evaluated. The prediction algorithm makes use of three main data structures Trace Record Matrix (*TRM*), Path Database (*PD*) and Historical Path Database ( $D_x^H$ ). The prediction is valid and useful only for a specified period of time and for a number of cells that are likely to be likely crossed. In general, the more cells considered in the prediction, the better the obtained approximation will be, but with a higher expense of the required computational resources. For a second comparison, we considered a single-step prediction scheme [11], belonging to Lempel-Ziv algorithms; in particular we considered the Active LeZi scheme (ALeZi) [34], which shows the higher hit-rate in prediction, if the PPM scheme is coupled with it. In [11], [34] the way the ALeZi scheme builds the prediction tree is described. In order to apply this scheme, for each  $c_i \in C$  a symbol  $s_i$  (cell identifier) has been defined, obtaining the set  $S$  of the available symbols. The probability calculation is based on PPM algorithm, observing the previous ( $k-1$ ) symbols in order to predict the  $k$ -th one. Regarding our scheme, the MUX algorithm was considered to be active, with a compression factor  $cf=0.4$  (as can be seen from simulations, this value represents a good trade-off for the obtained performance: system utilization maintains higher than 90%, prediction error has a mean value of about 0.12, CBP assumes the average value of 0.1 while CDP maintains below 0.11 in the average). While the ALeZi scheme considers only the most suitable next cell, DPBMA and UMP profiles are able to predict more than one cell for each hand-over. The cases of 1, 2 and 3 cells for next hand-over events were considered for both DPBMA and UMP.

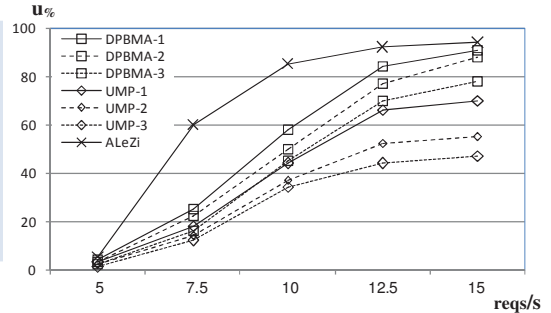


Fig. 25. Comparison of DPBMA, UMP, ALeZi in terms of utilization.

In fig. 25, the comparison, in terms of system utilization, among the proposed scheme and the considered ones is proposed, varying the CAR. It is possible to observe how the ALeZi scheme outperforms the other ideas, only because it provides one predicted cell for each step, so it does not take into account the CHT and only the next cell is considered. Passive reservations are not present in the ALeZi scheme, so no bandwidth wastage is introduced into the system. The slight degradation in utilization for the ALeZi scheme is due to the normal overhead of the MRSVP protocol, which wastes communication channels for signalling protocol messages. In addition, the DPBMA offers acceptable results. For

increasing values of CAR, it offers better performance for the reasons explained before and, in all the cases, it outperforms the UMP. In particular, for high CAR values, there is a gap higher than 22% between DPBMA and UMP, thanks to the multiplexing scheme. Figure 26 illustrates the comparison among the schemes in terms of average prediction error. The increasing trend for higher CARs is due to the higher presence of passive reservations: even if the predictor fails to chose the right cell, there will be a lower chance to find available bandwidth, due to the higher presence of passive reservations. It can be seen that the ALeZi scheme offers the higher value (no passive reservations are made). In this case, DPBMA outperforms UMP and ALeZi for all the cases (1, 2 or 3 predicted next cells).

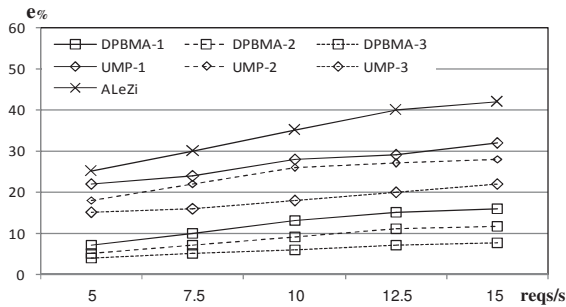


Fig. 26. Comparison among DPBMA, UMP and ALeZi in terms of average prediction error.

In fig. 27, the schemes are compared in terms of CBP: first of all, it can be observed that the ALeZi prediction algorithm cannot guarantee service continuity since it is able to predict a next cell step-by-step, while the others can make a totally in-advance prediction of all the future cells that will be visited.

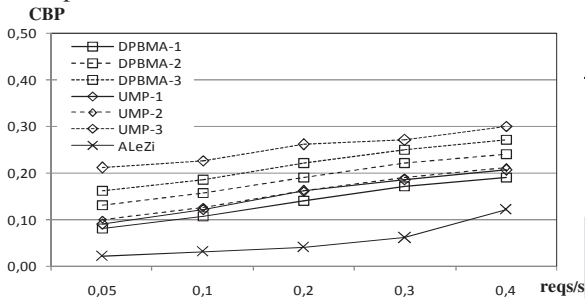


Fig. 27. Comparison among DPBMA, UMP and ALeZi in terms of CBP.

It is clear that the considered Active Lempel-Ziv scheme offers a low CBP, since the call admission control is made only on two cells. This time the performance of DPBMA and UMP are comparable, with an average gap of about 0.04. Figure 28 illustrates the obtained results in terms of CDP. Also in this case, ALeZi is unsuitable, because it presents too high values for QoS and service continuity purposes. The probability of finding available resources for each hand-over is very low, so the calls are often dropped, especially for high CARs. The performance of UMP and DPBMA are never comparable. In general, DPBMA offers better results, with an average gain of about 10%. In the worst case (1 predicted next cell, high CAR) the CDP stays below 0.15. The final figure of the paper illustrates a graphical representation of the committed prediction error for each cell. Given that all the statistics average the results for the whole set of cells, the main aim of fig. 29 is to represent how the prediction error is distributed over the map. It is possible to see how the error

percentages reflect the average values calculated in the previous statistics.

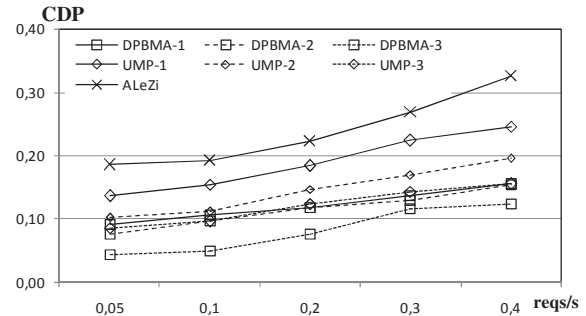


Fig. 28. Comparison among DPBMA, UMP and ALeZi in terms of CDP.

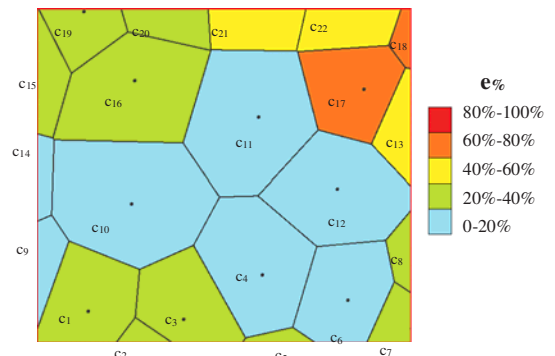


Fig. 29. Graphical representation of the way the prediction error is distributed among the system cells.

On the upper right corner the error is higher than the one of the other places because the set of cells  $C_{13}, C_{17}, C_{18}, C_{21}, C_{22}$  cover a bigger urban area, so the probability of taking different roads is higher. In the other cases, the error stays under 16% or 22%.

## V. CONCLUSIONS

This work proposes a new distributed Markovian prediction scheme for wireless cellular networks with vehicular mobility, integrating the passive reservation and multiplexing policies. It is also based on a road discretization algorithm, guaranteeing service continuity in QoS networks, without disrupting system utilization performance. The idea is independent from the considered coverage technology (UMTS, WLAN, GSM), as well as from the mobility model and it is of general application. The strength of the proposed distributed idea resides in the integration of the Markov predictor and the time multiplexing scheme, leading to DPBMA, which offers very good performance in terms of prediction error, utilization, CBP and CDP. The proposed integrated idea was compared with two existing works and it has shown better results, especially in terms of system utilization and CDP. In particular, after many considerations regarding performance and complexity, we highlighted that that a compression factor of 0.4 can reduce the number of computations of the Markov model, ensuring good performance results.

## ACKNOWLEDGEMENT

The authors would like to thank Mr. Andrea Lampasi and Dr. Francesco Strangis for their efforts and help in collecting coverage data and implementing graphical interfaces.

## REFERENCES

- [1] X. Fu, S. Henning, Bader A., Hogrefe D. (2005, Oct.). NSIS: a new extensible IP signaling protocol suite. *IEEE Comm. Magazine*. 43(10), pp. 133-141.
- [2] Q. Huang, G.S. Kuo, "Dynamic RSVP extension for wireless mobile IP networks," in *Proc. IEEE VTC*, 2004, Vol.4, pp. 2683-2687.
- [3] F. De Rango, P. Fazio, S. Marano. (2009, Mar.). Utility-based predictive services for adaptive wireless networks with mobile hosts. *IEEE Trans. on Vehicular Technology*, 58(3), pp. 1415-1428, 2009.
- [4] F.J. Martinez, J.C. Cano, C.T. Calafate, P. Manzoni, "CityMob: A mobility model pattern generator for VANETS", in *Proc. IEEE ICC*, 2008, pp. 370-374.
- [5] H. Si, Y. Wang, J. Yuan, X. Shan, "Mobility Prediction in Cellular Network Using Hidden Markov Model", in *Proc. IEEE CCNC*, 2010, pp. 1-5.
- [6] Y. Chon, E. Talipov, H. Shin, H. Cha. (2014, Mar.). SmartDC: Mobility Prediction-Based Adaptive Duty Cycling for Everyday Location Monitoring. *IEEE Trans. on Mobile Computing*, 13(3), pp. 512-525.
- [7] C.F. Wu, L.T. Lee, H.Y. Chang, D.F. Tao. (2011). A Novel Call Admission Control Policy Using Mobility Prediction and Throttle Mechanism for Supporting QoS in Wireless Cellular Networks. *Journal of Control Science and Engineering*.
- [8] Y.B. Lin, C.C. Huang-Fu, N. Alrajeh. (2013, Jun.). Predicting Human Movement Based on Telecom's Handoff in Mobile Networks. *IEEE Trans. on Mobile Computing*, 12(6), pp. 1236-1241.
- [9] I.F.Akyildiz, W.Wang. (2004, Dec.). The Predictive User Mobility Framework for Wireless Multimedia Networks. *IEEE/ACM Trans. on Networking*, 12(6), pp.1021-1035.
- [10] L. Velmurugan, P. Thangaraj. (2012). A Hidden Genetic Layer Based Neural Network for Mobility Prediction. *American Journal of Applied Sciences*. 9(4), pp.526-530.
- [11] A.R. Carrion, C. Garcia-Rubio, C. Campo. (2010, Aug.). Performance Evaluation of LZ-Based Location Prediction Algorithms in Cellular Networks. *IEEE Comm. Letters*. 14(8), pp. 707-709.
- [12] D. Katsaros, Y. Manolopoulos. (2009, Apr.). Prediction in wireless networks by Markov chains. *IEEE Wireless Communications*. 16(2), pp. 56-64.
- [13] *Location prediction algorithms for mobile wireless systems Wireless Internet Handbook*, CRC Press Inc., FL, USA, Cheng-Jain-Van Den Berg, pp. 245-263.
- [14] L. Song, D. Kotz, D. Jain, R. He, X. (2006, Dec.) Evaluating Next-Cell Predictors with Extensive Wi-Fi Mobility Data. 5(12) *IEEE Trans. on Mobile Computing*, pp.1633,1649.
- [15] F. De Rango, P.Fazio, S.Marano, (2006, Nov.) Cell Stay Time Analysis under Random Way Point Mobility Model in WLAN Networks. 10(11) *IEEE Communication Letters*, pp.763-765.
- [16] F. De Rango, P.Fazio, S.Marano, "Mobility Prediction and Resource Reservation in WLAN Networks under a 2D Mobility Models," in *Proc. VTC*, 2006, pp. 1-5.
- [17] P. Fazio, M. Tropea, (2012). A New Markovian Prediction Scheme for Resource Reservation in Wireless Networks With Mobile Hosts. 10(4) *AEEE*, pp.204-210.
- [18] M.R. Bhalla, A.V. Bhalla, (2007, Aug.) Generations of Mobile Wireless Technology: A Survey. *International Journal of Computer Applications*, Vol. 5 (4), pp. 26-32.
- [19] CISCO, "802.11ac: The Fifth Generation of Wi-Fi", Technical White Paper, 2014.
- [20] P.Fazio, F. De Rango, S.Marano, "2D Movement Direction-Based Reservation Scheme for WLAN Clusters with Passive Advanced Reservations" in *Proc IEEE CCECE*, 2008, pp. 1663-1666.
- [21] Landstrom, A., Jonsson, H., Simonsson, A., "Voronoi-Based ISD and Site Density Characteristics for Mobile Networks", in *Proc IEEE VTC Fall*, 2012, pp. 1-5.
- [22] A.E. Baert, D. Seme, "Voronoi mobile cellular networks: topological properties," in *Proc. IEEE ISPDC*, 2004, pp. 29-35.
- [23] Ullah R., Faisal N., Safdar H, Maqbool W., "Voronoi cell geometry based dynamic Fractional Frequency Reuse for OFDMA cellular networks", in *Proc IEEE ICSIPA*, 2013, pp. 435 - 440.
- [24] F. De Rango, P.Fazio, S.Marano, "Cell Stay Time Prediction for Mobility Independent Predictive Services in Wireless Networks," in *Proc. IEEE WCNC*, 2005, pp.1792-1797.
- [25] G. Shivaram, G. Seetharaman, T.R.N. Rao, "Data compression of discrete sequence: a tree based approach using dynamic programming", in *Proc. SIAM - ACM*, 1997.
- [26] V. Zeimpekis, P. Kourouthanassis, G. Giaglis, "Mobile and Wireless Positioning Technologies", in *Telecommunication Systems and Technologies*, EOLSS Publishers Co Ltd, Vol. 6 (108), 2007.
- [27] Sherif Akoush and Ahmed Sameh, "Mobile User Movement Prediction Using Bayesian Learning for Neural Networks", in *Proc. ICSNC*, 2007, pp.191-196.
- [28] J.G. Andrews, H. Claussen, M. Dohler, S. Rangan, M.C. Reed, (2012) Femtocells: Past, Present, and Future. *IEEE Journal on Selected Areas in Communications*, Vol. 30 (3).
- [29] M.I. Jordan, "Graphical Models", in *Statistical Science*, vol. 14, issue 1, The Institute of Mathematical Statistics, 2004, pp.140-155.
- [30] G. E. P. Box and Mervin E. Muller, (1958). A Note on the Generation of Random Normal Deviates. 29(2) *The Annals of Mathematical Statistics*, pp. 610-611.
- [31] S. Ross, "A First Course in Probability", *Probability Textbooks*, 8ed, Prentice Hall, Pearson, 2010, pp. 279-281.
- [32] R.K. Jain, D.W. Chiu, W.R. Hawe, "A Quantitative Measure of Fairness and Discrimination for Resource Allocation in Shared Computer System", DEC Research Report TR-301, 1984.
- [33] D. Montgomery, G.C. Runger, "Applied Statistics and Probability for Engineers", 5th ed., Hoboken, 2003.
- [34] K. Gopalratnam and D. J. Cook, (2007, Jan.-Feb.) Online sequential prediction via incremental parsing: the active LeZi algorithm. 22(1) *IEEE Intelligent Systems*, pp. 52-58.
- [35] Cisco Systems, "Wi-Fi Location-Based Services 4.1 Design Guide - Chapter 2: Location Tracking Approaches", 2008.



**Peppino Fazio** graduated in Computer Science Engineering (M.D.) in May 2004, at the University of Calabria (Italy). He took the Ph.D. in Electronics and Communications Engineering at the same University in January 2008. In the same year he spent a period of six months at the UPV of Valencia (Spain), for researching about VANET architecture. He is currently assistant professor at DIMES Department of University of Calabria, after many

international collaborations. He is peer reviewer and TPC member of different international conferences, as well as for many international journals, such as IEEE TVT, COMMLET, VTM, SPRINGER TELS, MONET, ELSEVIER VEHCOMM, COMNET, SIMPAT, JESTCH. His research interests include mobile communication networks, QoS architectures and interworking wireless and wired networks, mobility modeling for WLAN environments and mobility analysis for prediction purposes. He published more than 75 papers among International Journals, Conferences and Book Chapters.



**Mauro Tropea** was born in 1975 and graduated in computer engineering at the University of Calabria, Italy, in 2003. Since 2003 he has been with the telecommunications research group of DIMES. in the University of Calabria. In 2004 he was awarded a regional scholarship on Satellite and Terrestrial broadband digital telecommunication systems. His research interests include

satellite communication networks, QoS architectures and interworking wireless and wired networks, mobility models and vehicular issues.



**Floriano De Rango** graduated in Computer Science in October 2000, and a Ph.D. in electronics and telecommunications engineering in January 2005, both at the University of Calabria, Italy. From January 2000 to October 2000 he worked in the Telecom Research LAB C.S.E.L.T. in Turin with a scholarship. From March 2004 to November 2004 he was visiting

researcher at the University of California at Los Angeles (UCLA). He is now Assistant Professor at DIMES Department, University of Calabria. He was recipient of the Young Researcher Award in 2007 and he is reviewer and TPC member for many International Conferences and reviewer for many journals such as IEEE Communication Letters, JSAC, IEEE Trans. on Vehicular Technology, Computer Communication, Eurasip JWCN, WINET etc. His interests include Distributed Wireless Networks, Internet of Things, Adaptive Wireless Networks, Ad Hoc and Sensor Networks, Pervasive Computing, Satellite networks, IP QoS architectures. He published more than 180 papers among International Journal and Conferences. He founded two startups working in the field of Internet of Things and Wireless Advanced Broadband Telecommunication Systems. One of his startup "Spintel srl" ([www.spintel.it](http://www.spintel.it)) has been awarded by Intel as one of the best 20 promising startup in Europe in the Intel Business Challenge Competition in 2013.



**Miroslav Voznak** born in 1971 is an associate professor with the Department of Telecommunications, Technical University of Ostrava, Czech Republic and foreign professor with Ton Duc Thang University in Ho Chi Minh City, Vietnam. He received his Ph.D. degree in telecommunications in 2002 at the Technical University of Ostrava. He is a senior researcher in the Supercomputing center IT4Innovations in Ostrava, Czech Republic, a member of

editorial boards of several journals and a member of many boards of conferences supported by IEEE such as TSP, INBIS, CN, etc. Topics of his research interests are IP telephony, wireless networks, speech quality and network security.

DRAFT